Design of Robust Autoland Control Laws using μ-Synthesis

G.H.N. Looye*, C.E.S. Sancho†, A.A. Makdoembaks‡ and J.A. Mulder§

Delft University of Technology
Faculty of Aerospace Engineering
Control and Simulation Group
Kluyverweg 1, 2629 HS Delft
The Netherlands

*German Aerospace Center
DLR-Oberpfaffenhofen
Institute for Robotics and Mechatronics
D-82234 Wessling
Germany

E-mails: gertjan.looye@dlr.de, c.e.s.sancho@student.tudelft.nl,
amil.makdoembaks@asml.com, j.a.mulder@lr.tudelft.nl

Abstract

The design of autoland control laws for a large civil transport aircraft using μ-synthesis is discussed. The controller architecture consists of functions for tracking the ILS-approach path, and for flare and alignment of the aircraft shortly before touchdown. For each function, design requirements are formulated using weighting functions in the frequency domain. Model uncertainty is incorporated via automatically generated Linear Fraction Parametric Uncertainty Models (LF-PUMs). The structured singular value, as the measure for robust performance, is then optimized via so-called D-K iteration. Robustness of the resulting controller functions is assessed via μ-analysis and batch simulations. Monte Carlo analysis is used to test autoland performance under varying environment and disturbance parameters. As an ultimate robustness test, this analysis is performed with the nominal, as well as worst-case aircraft model configurations. The reason for this is, that in practice the Monte Carlo aircraft model may be more detailed and accurate than the model available during the design, frequently requiring late additional design iterations.

1. Introduction

The design and certification of control laws for Cat-III automatic landings is a very demanding task. The automatic landing mission itself, consisting of final approach path tracking using the Instrument Landing System (ILS) and flare / runway alignment (in case of cross wind) shortly before touch down, is relatively simple. However, autoland system design is complicated by the large amount of varying and uncertain parameters involved. These can be divided into environment parameters (called p_e in this paper), aircraft loading and configuration (known) parameters (p_a), and uncertain aircraft model parameters (p_u). Environment parameters include for example runway, approach terrain, wind and atmospheric characteristics, see figure 1. Uncertain aircraft model parameters are for example tolerances on aerodynamic and inertia coefficients.

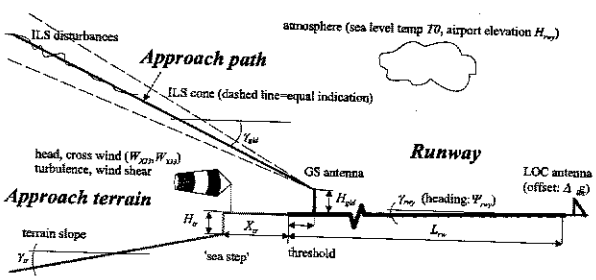

Figure 1: Typical parameters for a landing case

A typical design process for autoland control laws is depicted in figure 2. As a first step, the global control law architecture is defined, based on functional design requirements for the autoland mission (block A). An autoland controller usually consists of several functions, such as the glide slope and flare mode. Detailed design and synthesis of these functions is performed in blocks B, after which these are integrated into the autoland controller structure (block C). The control laws are extensively tested under varying parameter com-

*Research Engineer DLR, PhD candidate
†Former graduate student, TU-Delft
‡Former graduate student, TU-Delft
§Professor, head of the Control and Simulation Division

binations in face of the design and certification specifications (block D). When specifications are not met, the controller functions involved need to be adjusted (loop 1 in figure 2), or, in case of severe shortcomings, the over-all architecture may have to be reconsidered (loop 2).

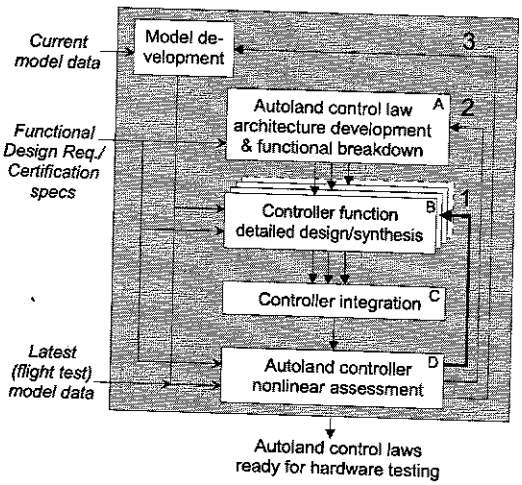

Figure 2: Autoland control laws design process

Certification of autoland control laws is based on extensive Monte Carlo (MC) analysis (performed in block D), in which a large number of landings is simulated with randomly selected parameter vectors p_a and p_e (not p_u). Based on statistics of landing parameters, such as touchdown and sink rate dispersions, the risk of exceeding specific limits is assessed.

For MC analysis, a high-fidelity aircraft model is used and the results have to be validated with a considerable number of flight tests. The aircraft model that is employed for control law design (top left in figure 2) usually has lower fidelity. First of all, in the earlier design stages the available data is not as accurate as during final Monte Carlo assessment for certification, introducing considerable uncertainty (eg. parameters p_u) in the design model. Second, simplifications may have to be made, in order to make the design model tractable for controller synthesis.

In the ideal case, the controller design based on the lower fidelity design model would pass the MC assessment based on the high-fidelity model, and flight testing, in one shot. Unfortunately, additional late (and therefore costly) design iterations are usually required with an updated design model (loop 3 in figure 2). The expectation is that these iterations can be avoided to a large extent, in case uncertainties are explicitly addressed in the synthesis of the controller functions (blocks B). *The objective of the work described in this paper, is to investigate to what extent the application of a robust control method may help to achieve this.*

A promising robust control methodology is μ-synthesis [14], which directly aims at optimizing robust performance by minimizing the structured singular value μ. Performance objectives are formulated using weighting functions in the frequency domain. Uncertainty on model parameters is incorporated in a feedback interconnection in a so-called Linear Fractional Parametric Uncertainty Model (LF-PUM).

The design in this paper is performed along the lines of figure 2. μ-Synthesis is applied in blocks B, to design the controller functions of the autoland system. As final assessment, Monte Carlo analysis (block D) is performed with the available aircraft design model. In order to represent differences between the design model and MC model in practice, the assessment is performed with nominal as well as worst case uncertain model parameter combinations (p_u). This helps to interpret the actually achieved robustness of a μ-synthesis design that is subject to realistic performance objectives.

This paper is structured as follows. In section 2 the aircraft model is described, in section 3 μ-theory is reviewed. The development of LF-PUMs is discussed in section 4. In section 5 the controller architecture is described. Section 6 discusses the design of controller functions using μ-synthesis. In section 7 controller performance and robustness are evaluated, and in section 8 conclusions are drawn.

2. The aircraft model

The nonlinear aircraft model is based on the Newton-Euler equations of motion [15] for a rigid body and represents a large civil aircraft with two turbofan engines (see also ref. [11]). The aerodynamics are valid for the landing configuration and include ground effect. Aerodynamic coefficients as well as the moments of inertia have tolerances of 10% (longitudinal parameters) or 30% (lateral parameters, ground effect). For example, the tolerance on the derivative of the aerodynamic pitching moment coefficient C_m with respect to the pitch rate q is written as:

$$C_{m_q} = C_{m_{q0}}(1 + \Delta C_{m_q}) \qquad (1)$$

where $C_{m_{q0}}$ is the nominal value, and ΔC_{m_q} is the tolerance (which is an element of the vector p_u).

The controls available to the controller are ailerons δ_A, elevator δ_E, rudder δ_R, and pressure ratios in both engines $\delta_{EPR1,2}$. The control surface actuator models are linear, but rate and position limited. The nonlinear engine dynamics and thrust models are based on look-up tables.

The wind model includes wind shear as present in the earth's boundary layer, Dryden turbulence filters (as specified in [8]), as well as additional parameterized wind shear models. For the atmosphere, approach terrain, runway and ILS equipment characteristics, parameterized (parameter vector p_e) models are included according to [8].

The model outputs are the measurements available to the control system: calibrated airspeed V_{cas}, true airspeed V_{tas}, ground speed V_g, body angular rates p, q, r, attitude angles ϕ, θ, ψ, load factors n_x, n_y, n_z, flight path angles χ, γ, angle of attack α, vertical speed V_Z, deviations from the ILS beam $\epsilon_{LOC}, \epsilon_{GS}$ (in mA), and radio and barometric altitude H_{ra}, H_{baro}, The aircraft mass m, and the center of gravity location x_{CG} ($\in p_a$) may be assumed known. The sensor dynamics models are linear. The signals ϵ_{LOC} and ϵ_{GS} are corrupted with noise.

3. Review of μ-synthesis

The controller synthesis and analysis problem in its most general form is shown in figure 3 [14].

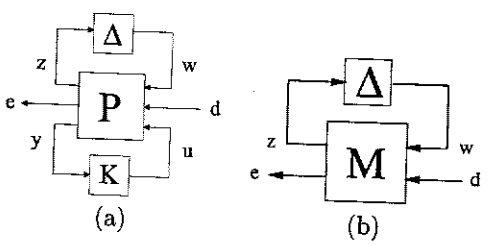

Figure 3: (a) General Analysis and Synthesis framework, (b) same system, with P and K included in M

The generalized system P has three input/output pairs: y and u (measurements and control inputs from the controller K), e and d (performance signals and external inputs respectively), and z and w through which unit-norm perturbations in Δ are fed back into the system.

Given the controller K, which might be obtained from any synthesis method, the generalized closed loop system for analysis as depicted in figure 3(b) is $M(s)$.

Performance robustness of the system $M(s)$ is then characterized by the transfer function from d to e, which depends on the perturbation $\Delta(s)$ in the form of a Linear Fractional Transformation (LFT):

$$\frac{e}{d} = M_{22} + M_{21}\Delta[I - M_{11}\Delta]^{-1}M_{12} \qquad (2)$$

(Laplace variable s has been omitted) Eq. 2 reveals that M_{11} imposes robust stability, since the fractional part may become singular for some $\Delta \in \mathbf{\Delta}$. Well-definedness of (2) can be assessed along the frequency axis using the structured singular value μ [14]:

$$\mu_{\mathbf{\Delta}}[M(j\omega)] := \frac{1}{\min\{\bar{\sigma}(\Delta(j\omega)):\Delta\in\mathbf{\Delta},\det(I-M(j\omega)\Delta(j\omega))=0\}} \qquad (3)$$

In words $\mu_{\mathbf{\Delta}}$ is the reciprocal of the smallest $\Delta(j\omega)$ (where we use $\bar{\sigma}$ as the norm) we can find in the set $\mathbf{\Delta}$ that makes the matrix $I - M(j\omega)\Delta(j\omega)$ singular. If no such Δ exists, $\mu_{\mathbf{\Delta}}$ is taken to be zero. If M is stable, the following theorems apply [14]:

1. **Nominal performance is satisfied if and only if**
$$\|M_{22}(j\omega)\|_\infty < 1 \qquad (4)$$
2. **Robust stability is satisfied if and only if**
$$\mu_{\mathbf{\Delta}}[M_{11}(j\omega)] < 1 \quad \forall\,\omega \qquad (5)$$
3. **Robust performance is satisfied if and only if**
$$\mu_{\mathbf{\Delta_e}}[M(j\omega)] < 1 \quad \forall\,\omega \qquad (6)$$

Where the augmented perturbation $\Delta_e = \mathrm{diag}(\Delta, \Delta_p)$ is connected around the system M (Δ_p is a fictitious full complex perturbation matrix).

To synthesize a controller that achieves robust performance, we need to minimize $\mu_{\mathbf{\Delta_e}}[M]$. This is done by minimizing an upper bound [2]:

$$\inf_K \inf_D \| DM(P,K)D^{-1} \|_\infty$$

where D is a scaling matrix with structure depending on $\mathbf{\Delta_e}$. The problem is solved iteratively: holding D constant, we have an H_∞ optimization problem [5], while holding K constant, the optimization problem is convex in $ln(D)$. This iteration is not guaranteed to converge, but usually works well. Since real-valued and repeated parameters in Δ are addressed as complex and independent, the optimized upper bound may be conservative. For a more thorough treatment of the theory outlined above, see refs. [17, 13].

4. Development of LF-PUM models

In order to incorporate an aircraft model with its parametric uncertainties p_u into the interconnection structure depicted in figure 3(a), it is necessary to formulate this model in LFT form as well, called Linear Fraction Parametric Uncertainty Model (LF-PUM). For this work, the LF-PUM could be generated automatically from the nonlinear aircraft model. This model has been developed in the object-oriented modeling environment Dymola [6], using the DLR Flight-Dynamics library [12]. Using Dymola, symbolic differential equations of the model are generated. Via symbolic linearization and substitution of trim values for the state and input vectors, the following linear model is obtained [16]:

$$\delta\dot{x} = A(p_u)\delta x + B(p_u)\delta u \quad (7)$$

$$\delta y = C(p_u)\delta x + D(p_u)\delta u \quad (8)$$

where δ denotes small perturbations from the trimmed condition. Since the dependencies on the parameters p_u are rational (eq. 1), this state space realization can be automatically transformed into an LFT, using the Parametric Uncertainty Modeling (PUM) toolbox [9]. Separate LF-PUM descriptions for lateral and longitudinal dynamics have been generated. The algorithms in the PUM toolbox heavily rely on reduction of multi-dimensional systems, sometimes still resulting in high order LF-PUM descriptions. The resulting matrices Δ for the longitudinal and lateral dynamics are:

$$\begin{aligned}\Delta_{lon} &= diag\,(\Delta C_D I_2, \Delta C_{Lt} I_4, \Delta\tfrac{d\epsilon}{d\alpha} I_7, \Delta\mu_{gr} I_7, \\ &\quad \Delta C_{m0} I_2, \Delta C_{mq}, \Delta C_{m\delta_e}, \Delta I_{yy}) \\ \Delta_{lat} &= diag\,(\Delta C_Y, \Delta C_{l0}, \Delta C_{n0}, \Delta C_{lp}, \Delta C_{lr}, \\ &\quad \Delta C_{np}, \Delta C_{nr}, \Delta C_{l\delta_a}, \Delta C_{l\delta_r}, \Delta C_{n\delta_a}, \\ &\quad \Delta C_{n\delta_r}, \Delta I_x, \Delta I_z, \Delta I_{xz} I_2)\end{aligned} \quad (9)$$

where for example $\Delta C_D I_2$ represents the tolerance on the drag coefficient C_D, which is repeated twice on the diagonal of Δ_{lon}. All longitudinal parameters are normalized according to their assumed bounds of 10%, the ground effect parameter μ_{gr} and the lateral parameters are scaled to 30%.

5. Controller architecture (A)

The autoland system design has been performed along the lines of figure 2. As a first step (block A), the over-all controller architecture as depicted in figure 4 was defined. Three main loops can be identified: Stability and Command Augmentation (SCA), Speed/Path Tracking (SPT), and Guidance. The lateral and longitudinal path tracking functions are used for approach path tracking, based on geometrical deviations that are estimated from localizer and glide slope signals in the LOC and GS modes respectively. The longitudinal SPT function also has to maintain the selected approach speed V_{app}. Thrust commands (T_c) generated by this function are transformed into Engine Pressure Ratio (δ_{EPR}) commands via an inverse thrust map.

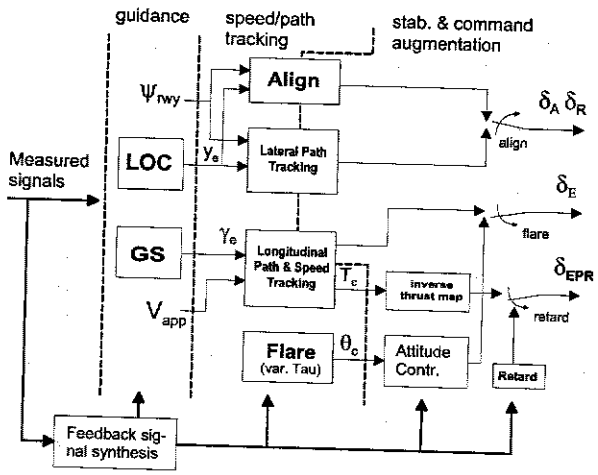

Figure 4: Autoland controller architecture (Remark: for block inputs, only command and error signals shown)

Shortly before touch down, the Flare, Retard, and Align functions are engaged. The align function controls lateral deviation y_e and aircraft yaw angle ψ, using the runway heading ψ_{rwy} as reference. The currently implemented flare mode is based on the variable Tau structure [10], which features low touch down dispersions under varying wind conditions. Pitch attitude behavior during flare plays an important role in pilot acceptance. For this reason, it was decided to control this variable in an inner loop (figure 4), allowing its behavior during flare to be shaped more easily.

Thrust retard is performed at a constant rate $\dot{\delta}_{EPR}$ (proportional to the ground speed at flare init), such, that the throttles reach idle position at touchdown.

Finally, in order to reduce the turbulence noise level in air data signals, complementary filtering between inertial and air data is applied in a Feedback Signal Synthesis function (figure 4).

The controller architecture (figure 4) shows a clear functional breakdown. The next step is the detailed design of the individual controller functions (blocks B in figure 2). The design approach for each individual function depends on the influence of the different types of varying and uncertain parameters (p_e, p_u, p_a, see section 1).

Uncertain aircraft model and aircraft configuration and loading parameters (p_u,p_a) directly influence aircraft dynamics and therefore performance and stability of the closed loop system. At this point, the tracking functions (pitch attitude inner loop, align, longitudinal and lateral path/speed tracking functions) are mostly affected. For this reason, these components are designed using μ-synthesis, which allows robustness to the uncertain parameters to be addressed in a highly structured way. Since scheduling of μ-synthesis control laws is not straight forward, it was decided to (conservatively) treat parameters p_a as uncertain parameters for now. In a future design, the intention is to compensate for the effect of varying p_a using a Dynamic Inversion inner loop [4, 1], or with the help of LPV techniques [7].

Environment parameters p_e (except for head and cross wind levels W_{X33} and W_{Y33}, see figure 1) mainly influence reference generation rather than tracking performance. These parameters are most effectively dealt with using complementary filtering [10, 11]. For example, a sloping runway (γ_{rwy} in figure 1) effectively changes the aircraft sink rate relative to the runway surface. The runway-referenced sink rate can be estimated by complementarily filtering of the radio altitude H_{ra} and inertial vertical velocity V_Z signals. The possible occurrence of a 'sea step' (H_{tr}), basically prohibits the use of the radio altimeter as a feedback signal, until the aircraft is close to the runway threshold.

The GS and LOC modes are most affected by environment parameters, and not by uncertain or known aircraft parameters. For this reason, these functions have classical structures.

The flare law is most sensitive to variations in all types of parameters, especially wind and turbulence. Having chosen a robust pitch attitude inner loop, proportional sink rate and altitude feed back in the variable Tau structure turned out to give most satisfactory results. However, it was realized that robustness to for example ground effect related uncertainty is not addressed in this way.

6. Design of controller functions (B)

The design process for controller functions using μ-synthesis is depicted in figure 5. It will be explained by example for the flare pitch attitude inner loop and align mode. The automatic generation of LF-PUMs (top left block) has been discussed in section 4.

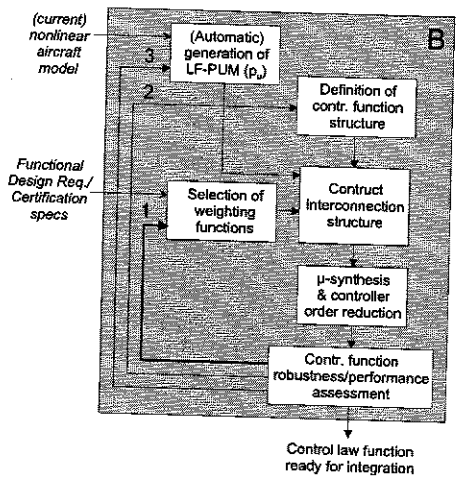

Figure 5: Control function design with μ-synthesis

Pitch attitude controller

Principal objectives for the design of the flare law inner loop arose iteratively in loop 1 in figure 2:
- use pitch controller to keep control over pitch attitude and avoid drops of the nose;
- avoid pitch overshoot at all cost;
- design for a fast response, i.e. small rise time;
- use preferably, inertial referenced signals to reduce sensitivity to noise and turbulence.

In a μ-synthesis design, performance specifications are reflected via frequency dependent weighting functions (figure 5). These are applied on signals of interest in the control loop. To this end, it is common practice to start the design with drawing an interconnection structure (central block in figure 5), see figure 6. The principal feedback loop consists of the aircraft LF-PUM (AC, Δ_{lon}), the controller K, sensor models H_{sens}, the first order actuator (bandwidth B_{act}), and a structural filter H_{str}. The latter was prescribed and had to be implemented with the controller. The principal task of the controller is pitch attitude tracking. The control input is elevator δ_E, the measurements are q and θ. The aircraft LF-PUM is generated around a trim point shortly before flare, where the

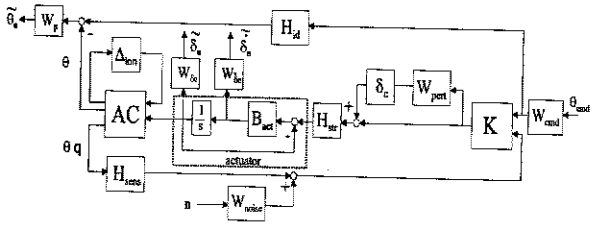

Figure 6: Interconnection structure for synthesis of the θ controller

ground effect is already influential ($h = 20\ m$, and $\gamma = -3°$).

In figure 6 a reference command is obtained from scaling the normalized reference θ_c with W_{cmd}:

$$W_{cmd} = 3\pi/180\ rad$$

The desired closed-loop command response behavior is reflected by the ideal model filter H_{id}. This filter turned out to be crucial for flare performance. After some trials (loop 1 in figure 5) the following weight was selected:

$$H_{id} = \frac{0.8^2}{s^2 + 2 \cdot 0.9 \cdot 0.8s + 0.8^2}$$

In order to impose the ideal command response behavior on the closed loop system, the difference between the output from and AC and H_{id} is weighted using W_p. At lower frequencies the error should be small, beyond the bandwidth of H_{id}, this can be relaxed. This is reflected in the weight by applying higher magnitude at lower frequencies:

$$W_p = \frac{3000}{W_{cmd}} \frac{\frac{1}{10}s + 1}{\frac{1}{0.002}s + 1}$$

The weight shows approximate integration up to a frequency of 10 rad/s, forcing the steady state error to be very small (i.e. $< 1/3000$). The location of the zero played a role in forcing controller roll-off. The weight W_p is multiplied with the inverse of W_{cmd}, so that the weighted error is relative to the command θ_c. Finally, in order to limit control activity, weights were applied on the elevator command and its rate:

$$W_{\delta_e} = \frac{1}{10}\frac{180}{\pi} \qquad W_{\dot{\delta}_e} = \frac{1}{20}\frac{180}{\pi}$$

The signal from the sensors (H_{sens}) may be corrupted by noise. This is reflected by adding filtered noise to the feed back signals using W_{noise}:

$$W_{noise_i} = 5 \cdot 10^{-6} \frac{\frac{1}{0.05}s + 1}{\frac{1}{0.5}s + 1}, \text{with } i = 1, 2$$

At low frequencies, the magnitude is kept low; the transfer function from $W_{noise}n$ to θ is a complementary sensitivity function which directly affects the error θ_e that is weighted by W_p.

The uncertainties in the model AC reflect tolerances on aerodynamic and inertia coefficients. In order to account for unspecified uncertainties such as time delays, unmodeled dynamics, etc., additional multiplicative uncertainty at the plant input is added. This is reflected using a normalized δ_c, and a frequency dependent scaling W_{pert}:

$$W_{pert} = 0.20 \frac{\frac{1}{3}s + 1}{\frac{1}{50}s + 1}$$

At lower frequencies, the error may be up to 20%, increasing from 3 rad/s up to a level of 50/3*0.2 *100%=333%. Additionally, this weight forces the controller to roll off at higher frequencies, preventing fast actuator activity.

For μ-synthesis (see figure 5), the interconnection structure in figure 6 is transformed into the generalized plant as depicted in figure 3(a). All uncertainty (Δ_{lon}, δ_c) is collected into the block Δ, the controller is in K, and the aircraft model, weighting functions, etc. are in the block P. Robust performance is now optimized via D-K iteration. As mentioned in section 3, due to limitations in the algorithms, real and repeated entries in the matrix Δ_{lon} have to be conservatively treated as complex and independent parameters. However, this did not turn out to pose severe problems. The resulting controller has order 54, which is reduced to 11 using balanced truncation [2].

During the design of a controller using μ-synthesis, performance and robustness assessment of intermediate results is mainly done via μ-analysis (in face of real-valued perturbations) and batch simulations (figure 5). Based on the results, weighting functions may be adjusted (loop 1), the controller structure may be reconsidered (loop 2), or the level of uncertainty may have to be adapted in case the balance shifts too much towards robustness (loop 3). Figure 7 depicts μ-analysis results based on the interconnection structure in figure 6, performed with respect to the real Δ_{lon} (eq. 9) and complex δ_c, and the final set of performance weights. Most importantly, robust stability (RS) is satisfied since the μ-plot stays below 1 for all frequencies (eq. 5). This implies that the system is stable for all uncertain parameter combinations. Nominal performance (NP) with respect to the selected weighting functions is almost satisfied (eq. 4), robust perfor-

mance (RP) is not satisfied (eq. 6). The latter is the objective that was (indirectly) optimized via D-K iteration. The achieved peak value of 1.48 means that the imposed performance requirements cannot be met for all uncertain parameter combinations. One measure to improve the μ-value is to design with a lower level of those uncertainties that mostly affect the synthesis (loop 3 in figure 5). However, stability robustness to the full range of uncertainty is then no longer incorporated. Furthermore, since nominal performance is practically achieved, the level of performance traded in for robustness (48 %) is considered acceptable.

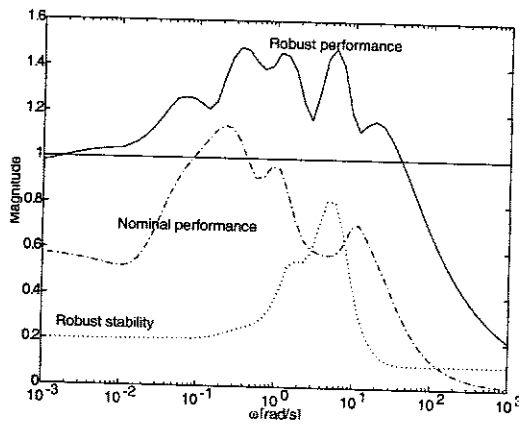

Figure 7: μ-Analysis of the pitch attitude controller

During the design, time responses are inspected continuously, in order to iterate on shaping the weighting functions (loop 1 in figure 5). This is not always straight forward, since typical criteria such as overshoot and rise time only translate indirectly. Time simulations for randomly selected parameter combinations are shown in figure 8. The result is satisfactory (no overshoot) and shows low sensitivity to model uncertainty.

Flare law

The flare law is shown in figure 9. A sink rate error is fed back via K_{FL}, which in this case has been scheduled as a function of p_a. The sink rate reference is generated from the deviation from the radio height with respect to a virtual reference that is at H_{bias} below the runway surface. The flare trajectory is exponential with a time constant τ. In order to obtain low touch down dispersions, the time constant is position, rather than time referenced. This is achieved by scaling τ with the ground speed [10]: $\tau = \tau_0(V_{g_0}/V_g)$. The flare law was tuned by hand.

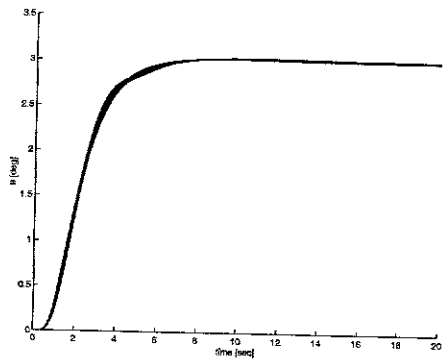

Figure 8: Nonlinear θ step responses for different Δ_{lon} combinations

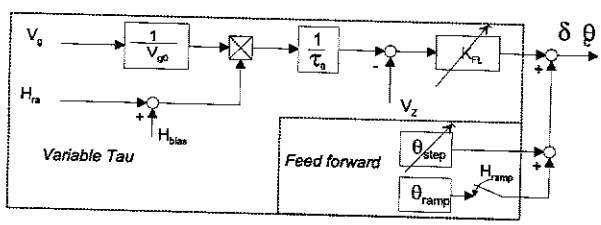

Figure 9: Flare law

The most important design constraints were a nominal touch down point near 400 m from the runway threshold, and a nominal sink rate of near 2.5 ft/s at touch down. Furthermore, for pilot acceptance reasons, pitch attitude may only rise, and the vertical acceleration may not change sign. The variable Tau structure turned out to have not enough degrees of freedom to satisfy these constraints. Furthermore, the ground effect heavily influences pitch attitude dynamics, in spite of tight inner loop control. For this reason, open loop commands as in figure 9 (θ_{step}, θ_{ramp}) were added. The parameters K_{FL} and θ_{step} were scheduled as a function of the mass and the center of gravity location. With help of the feed forward, all constraints could be met, except for the touch down point, which is nominally at 374 m. Flare initiation height h_{flare} was selected at 15 m.

Align controller

The interconnection structure for the align controller is depicted in figure 10. For this function, several configurations were tried (loop 2 in figure 5), such as separate ϕ, $\dot{\psi}$ and ϕ, ψ command tracking inner loops, but the combination of dY (lateral devisation from runway center line) and ψ gave best performance. The reference dY_{cmd} (= 0) is intended to keep lateral localizer deviation

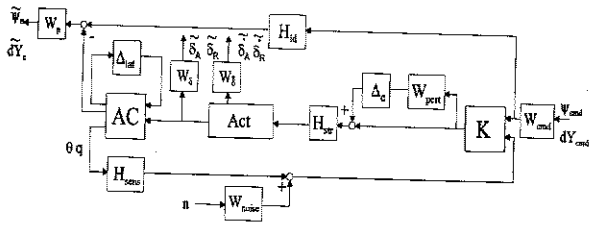

Figure 10: Interconnection structure for the synthesis of the dY/Ψ controller

small, while the aircraft heading is aligned with the runway center line via a ψ command. The controls used are aileron (δ_A) and rudder (δ_R). The controller inputs are dY_{cmd} (commanded offset from localizer), dY (offset from localizer), ψ_{cmd}, ψ, χ, p, r, ϕ. The command deviation and yaw angle are scaled using:

$$W_{cmd} = (W_{cmd_{dY}},\ W_{cmd_\psi})^T = (1,\ 2\frac{\pi}{180})^T$$

This weight is an important means to influence cross-coupling between the dY and ψ channels, see [3], and was determined iteratively (loop 1 in figure 5). The objectives of the weightings are very similar to those for the pitch attitude controller. The block AC now contains the lateral aircraft dynamics, the uncertainty Δ_{lat} contains lateral uncertain parameters as described in eq. 9. The complex uncertainty on the aileron and rudder inputs Δ_c are scaled with:

$$W_{pert_{ail}} = W_{pert_{rud}} = 0.1\frac{\frac{1}{3}s+1}{\frac{1}{100}s+1}$$

allowing a steady state error of 10%. The ideal models (in H_{id}) were chosen as:

$$W_{id_{dY}} = \frac{0.15^2}{s^2+2\cdot 0.9\cdot 0.15s+0.15^2}$$

for dY, and

$$W_{id_\psi} = \frac{0.3^2}{s^2+2\cdot 0.9\cdot 0.3s+0.3^2}$$

for ψ. The error weights are respectively:

$$W_{p_{dY}} = 200\frac{\frac{1}{5}s+1}{\frac{1}{0.0001}s+1}W^{-1}_{cmd_{dY}}$$

and

$$W_{p_\psi} = 4100\frac{\frac{1}{7}s+1}{\frac{1}{0.01}s+1}W^{-1}_{cmd_\psi}$$

The weights on actuator deflections and rates are:

$$W_{\delta_A} = W_{\dot{\delta}_A} = \frac{1}{40}\frac{180}{\pi},\quad W_{\delta_R} = W_{\dot{\delta}_R} = \frac{1}{20}\frac{180}{\pi}$$

Finally, the sensors outputs are corrupted with a noise level of $W_{noise} = 10^{-5}$.
Again, μ-synthesis was performed via D-K iteration, resulting in a controller with order 80, which was reduced to 25 using balanced truncation.
The lateral deviation dY in the align controller is obtained from the localizer signal, which may be corrupted with noise. In order to improve signal quality, complementary filtering is applied:

$$dY = \frac{\Delta Y}{\tau s+1} + \frac{\tau \dot{Y}}{\tau s+1}$$

where ΔY is the lateral deviation computed from the localizer signal, $\dot{Y}$ is estimated from: $V_g \sin(\chi - \psi_{rwy})$, and $\tau = 0.4$. Note that it is assumed that ψ_{rwy} is known exactly.

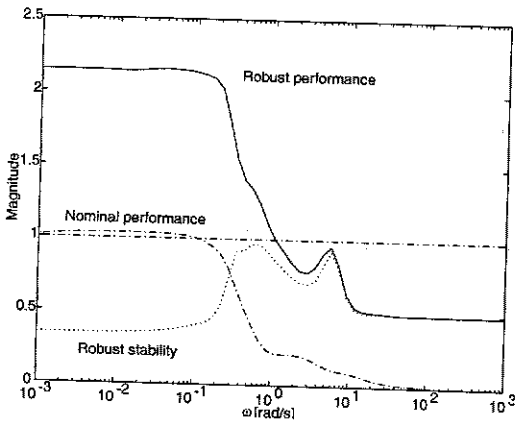

Figure 11: μ-Analysis of align controller

The μ-analysis plots for the align controller can be found in figure 11. The same conclusions can be drawn as for the pitch attitude controller. Note that performance considerably deteriorates due to uncertainty (RP $\sim$ 2.1). Closer analysis revealed that this is mainly caused by uncertainty in the lateral inertia coefficients. The effect is most apparant in decoupling between heading angle and lateral position tracking. This is illustrated in figure 12, showing nonlinear step responses to a heading (align) command for random combinations of uncertain parameters.

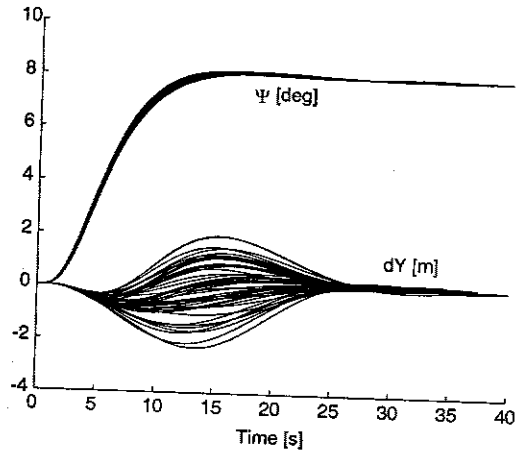

Figure 12: Nonlinear ψ step response for random combinations of uncertain parameters ($\psi_{cmd} = 8\ deg$).

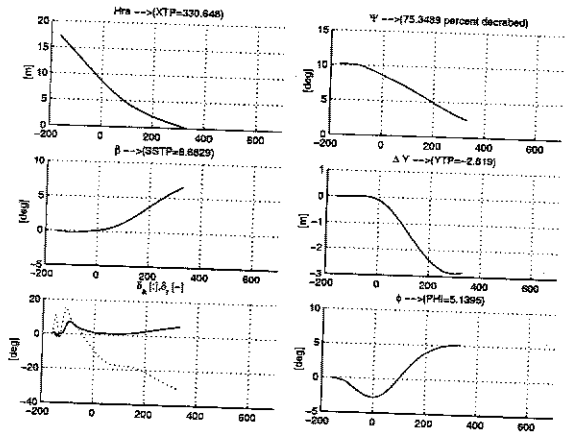

Figure 14: Nominal flare/decrab manoeuver with maximum cross wind

7. Controller assessment (D)

After integration of all designed functions (block C in figure 2), the performance of the completed autoland controller (figure 4) can be assessed (block D). First, in order to get an impression of the overall autoland system, a nominal landing simulation without wind, and one with 20 kts cross wind is performed, see figures 13 and 14 respectively.

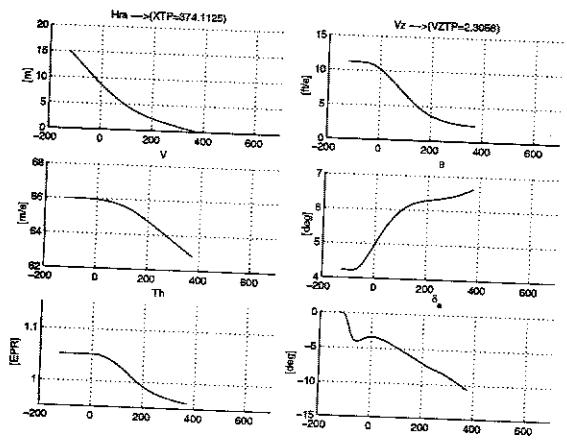

Figure 13: Nominal flare manoeuver

The touch down parameters such as sink rate and distance from threshold / center line are satisfactory, as well as pitch attitude behavior during flare and the amount of decrab in case of cross wind.
An important test for certification is Monte Carlo analysis (section 1). During MC analysis, 2000 landing simulations are performed with different combinations of aircraft loading and environment parameters (p_a, p_e). These parameters are selected randomly according to specified distribution functions [8]. After each simulation the landing gear height 60m from the threshold (HTP60), the longitudinal and lateral touch down points w.r.t. the threshold and center line (XTP, YTP), the sink rate (VZTP), the roll angle (PHI), and slip angle (SSTP) at touch down are determined. Assuming Gaussian distributions of the resulting variables, risks of exceeding specific limit values can be estimated via the associated cumulative distribution functions.
In this paper, only so-called average risk analysis results are shown (normally also limit risks have to be performed, in which one of the parameters is fixed to an extreme value). For certification, MC analysis is to be performed using a nominal, but high fidelity (flight test validated) aircraft model. In our case, only the simplified design model was available. In order to test if the control laws would still perform sufficiently in case the design and MC models differ (which may well occur in practice), we performed the analysis with the nominal (design) aircraft model, as well as six models with worst-case parameter vectors p_u. These worst-case combinations were found from simulations as shown in figures 13 and 14, by gridding parameters p_u between their maximum or minimum values. In this way, parameter vectors with worst PHI, HTP60, XTP, VZTP, SSTP, and YTP values were obtained.
The so-called cumulative distribution plots resulting from the seven (1 nominal, 6 worst-cases)

Monte Carlo analyses can be found in figure 15. In a subplot, each curve belongs to a worst-case parameter vector p_u. The end-points of the curves belonging to the nominal model have been marked with a star. As an example for interpretation, consider the plot for PHI (roll angle at touch down). The probability of landing with a roll angle of more than 10 degrees is 10^{-4}. Each curve should stay outside the colored areas, i.e. the risk value for PHI is 12 deg (left side of colored area), which means that the probability of landing at a higher roll angle may not be more than 10^{-8}. Since the nominal curve (marked with star) stays outside the shaded area, this risk is not exceeded. From the VZTP figure it can be seen that the risk of landing with a sink rate larger than the limit value is violated, even for the nominal model. This is mainly caused by the effect of turbulence. In

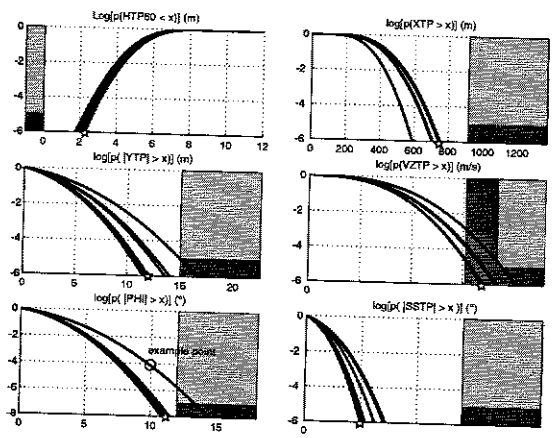

Figure 15: Cumulative distribution of the average risks for worst case uncertain model parameters

addition to the sink rate, the risk limits for lateral touch down location (YTP) and roll angle at touchdown (PHI) are not fulfilled in some model cases. In figure 12, the sensitivity of the heading step response (basically an align manoeuver) is considerably lower than for the associated response of dY. This correlates with the fact that the slip angle (SSTP) shows lower sensitivity and better performance than YTP in figure 15.

In order to interpret the results, it is helpful to compare the results with a reference controller, see figure 16. This controller nominally performs considerably better (curves indicated by star), but for the lateral risks, the spread of the curves is considerably larger, indicating larger sensitivity. Longitudinally, the reference controller is better, es-

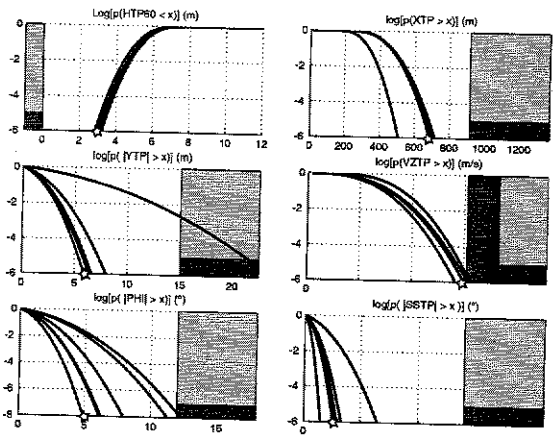

Figure 16: Cumulative distribution of the average risks for worst case uncertain model parameters, reference controller

pecially regarding VZTP. This may be caused by the fact that in the flare law, uncertainty was only considered in the pitch attitude inner loop design.

8. Conclusions

A successful automatic landing system design based on μ-synthesis was performed, with emphasis on handling uncertain model parameters. For the nominal case, the system nearly passes prescribed Monte Carlo average risks analysis. Fulfilling all criteria will require further enhancements in the controller architecture (see figure 2), and/or the amount of uncertainty may have to be reduced (see below).

Achievement of the objective to reduce model-related design iterations (loop 3), is hard to assess. In order to get some indication, MC analysis was performed with worst-case uncertain aircraft model parameters. Compared with a reference controller, lower sensitivity to model uncertainty has been achieved for lateral dynamics, where uncertainty had been addressed to full extent in the synthesis. For the flare, this was only done in the inner loop. Design of this function using μ-synthesis may improve robustness, but an effective way to impose constraints on pitch attitude behavior must be found.

Design specifications could be successfully translated into weighting functions in the frequency domain, but this required many iterations in loop 1

in figure 5, as well as in figure 2. For the present autoland problem, the application of μ-synthesis may not have reduced the amount of trial and error in achieving the performance objectives compared with a classical design.
The developed autoland system has a modular structure. The dynamic orders of the components that have been designed with μ-synthesis are relatively high (eg. 25 for the align function). The application of advanced order reduction algorithms may help to improve this. The specified tolerances on model parameters could be addressed directly in the μ-framework. However, the probability of uncertain parameter combinations to actually occur, can not be taken into account. For example, an offset of 30% on all lateral parameters is very unlikely to occur; a single parameter with this offset is quite likely however. As a consequence, more performance may have been traded in than actually necessary, and the performed analysis is too conservative. Therefore, future work will address reduction of uncertainty by taking probability of parameter combinations into account.

Acknowledgment

The design was based on the autoland benchmark developed within the EU-project Robust and Efficient Autopilot control Laws design (REAL), see also ref [11]. The extensively used Matlab-based Monte Carlo assessment tool SIMPALE was developed by REAL project partner ONERA, France.

References

[1] Richard J. Adams and Siva S. Banda. Robust Flight Control Design Using Dynamic Inversion and Structured Singular Value Synthesis. *IEEE Transactions on Control Systems Technology*, 1(2):80–92, June 1993.

[2] G. J. Balas, J. C. Doyle, K. Glover, A. Packard, and R. Smith. *μ-Analysis and Synthesis TOOLBOX, For Use with MATLAB*. The Math Works Inc., July 1993.

[3] S. Bennani and G. Looye. Design of Flight Control Laws for a Civil Aircraft Using μ-Synthesis. In *Proceedings AIAA-GNC conference 1998, Boston MA*. AIAA-98-4133.

[4] Samir Bennani and Gertjan Looye. Flight control law design for a civil aircraft using robust dynamic inversion. In *Proceedings of the IEEE/SMC-CESA98 Congress, Tunisia*, April 1998.

[5] J. Doyle, K. Glover, K. Khargonekar, and B. Francis. State-space solutions to standard h_2 and h_∞ control problems. *IEEE Transactions on Automatic Control*, 34:831–846, 1989.

[6] H. Elmqvist. Object-oriented modeling and automatic formula manipulation in Dymola. In *Scandinavian Simulation Society SIMS*, Kongsberg, Norway, 1993.

[7] A. Helmersson. Methods for robust gain-scheduling. PhD Thesis, Linköping University, Sweden, 1995.

[8] Joint Aviation Authorities Committee. Joint Aviation Requirements, All Weather Operations. Technical report, JAAC, 1996.

[9] Paul Lambrechts, Jan Terlouw, Samir Bennani, and Maarten Steinbuch. Parametric Uncertainty Modeling using LFTs. In *Proceedings of the American Control Conference, San Francisco, California*, pages 267–272, June 1993.

[10] A A. Lambregts. Avoiding the pitfalls in automatic landing control system design. *AIAA Paper 82-1599*, 1982.

[11] Gertjan Looye, Hans-Dieter Joos, and Dehlia Willemsen. Application of an Optimisation-based Design Process for Robust Autoland Control Laws. In *Proceedings of the AIAA Guidance, Navigation and Control Conference 2001, Montreal CA*, 2001.

[12] D. Moormann, P.J. Mosterman, and G. Looye. Object-oriented computational model building of aircraft flight dynamics and systems. *Aerospace Science and Technology*, 3(3), April 1999.

[13] Sigurd Skogestad and Ian Postlethwaite. *Multivariable Feedback Control*. Wiley & Sons, 1996.

[14] G. Stein and J. C. Doyle. Beyond singular values and loop shapes. *Journal of Guidance Control and Dynamics*, 14:5–16, 1991.

[15] Brian L. Stevens and Frank L. Lewis. *Aircraft Control and Simulation*. Wiley-Interscience Publication. John Wiley & Sons, Inc., New York, 1992.

[16] A. Varga, G. Looye, D. Moormann, and G. Grübel. Automated Generation of LFT-Based Parametric Uncertainty Descriptions from Generic Aircraft Models. Technical Report TP-088-36, GARTEUR, April 1997. available from `www.nlr.nl/hostedsites/garteur/sum36.html`.

[17] Kemin Zhou with John C. Doyle and Keith Glover. *Robust and Optimal Control*. Prentice Hall Inc., 1996.